Hindawi
Mathematical Problems in Engineering
Volume 2017, Article ID 6143054, 11 pages
https://doi.org/10.1155/2017/6143054

Research Article

Analysis of Contact Part of Error Tooth Surface and Dynamic Performance Prediction for Involute Gear

Xinrong Liu and Zhonghou Wang

School of Mechanical Engineering, University of Shanghai for Science and Technology, No. 516, Jungong Road, Yangpu, Shanghai 200093, China

Correspondence should be addressed to Zhonghou Wang; wang_zhonghou18@163.com

Received 11 August 2017; Revised 12 October 2017; Accepted 24 October 2017; Published 12 December 2017

Academic Editor: Yuri Vladimirovich Mikhlin

Aiming at the problem of constructing digital model of involute gear with error, the method of linear interpolation combined with area weight interpolation is proposed. Based on the non-feature discrete data block technique, the true tooth surface discrete data obtained by the coordinate measuring instrument is divided into blocks, and then the interpolation method is used to interpolate the nonmeasurement area to construct the real tooth surface with errors. The contact part and dynamic performance of the gear are predicted by using the constructed error tooth surface. The contact error of the tooth surface and the transmission error of the gear are verified by the test, and the reliability of the judgment result is judged by measuring the vibration in the direction of the gear meshing line. Compared with the example, this method not only reduces the computational complexity of the interpolation algorithm, but also improves the accuracy of the tooth interpolation data points and the smoothness of the error tooth surface.

1. Introduction

It is well known that the contact situation of the gears in the gearbox directly affects the gearbox's carrying capacity, vibration, and noise. The gear transmission error, the distribution area, and shape of tooth contact part have become an important index to measure the meshing performance of gear [1]. Due to gear manufacturing and installation errors, bearing clearance, load bearing parts' deformation, and so on, these factors will cause the gears to deviate from the ideal contact state. In order to accurately predict the dynamic performance of involute gears, the construction of error tooth surface is very important.

The reconstruction of complex surfaces is one of the most important research techniques in digital construction of tooth surface, and scholars at home and abroad have also done a lot of research about it. Lin et al. [2] assessed the large gear tooth profile deviation by using the NURBS (Nonuniform Rational B-Splines) surface. Zhang et al. [3] obtain digital tooth surface by using double three NURBS surfaces. And the tooth contact analysis of the digital tooth surface was carried according to the spatial meshing theory. Li et al. [4] construct the digital real model of hypoid gear aiming at the wear of tooth surfaces by using non-feature block interpolation technique. Sun et al. [5] propose an algorithm for constructing G1 continuous cubic triangular Bezier Surfaces from triangular mesh surfaces. In these studies, the detection of contact parts is mainly based on the traditional roll test and manual identification method. However, there are few studies about the contact surface of the tooth surface by the gear bearing contact analysis, and also there are studies about the prediction of meshing performance of the error tooth surface by contact part.

When the coordinate measurement is performed on the tooth surface, these methods are mainly applied to the smooth tooth surface because of the limited measurement data points of tooth surface. As for irregular tooth surfaces such as error tooth surfaces, the reason why the structural tooth surface can not reflect the true tooth surface is that most of the measurement data is separated from the structural tooth surface. In the above discrete data preprocessing technology, data segmentation is the bottleneck problem of constructing digital real tooth surface.

Based on the original research, an algorithm combining linear interpolation method with area weight interpolation method is proposed for constructing error tooth surface [6–10]. Besides, the digital construction of error tooth surface of involute gears is realized on the basis of NURBS surface. In this paper, the traditional smoothing algorithm is improved to ensure accuracy and increase the smoothness of digital tooth surface. The feasibility of the method proposed in this paper is verified by comparing the examples.

In contrast to constructing the digital model of single tooth surface, NURBS surface is used to construct the error tooth surface model of modified involute gears in this paper. Combined with the principle of involute gear meshing, the solution of the contact part of involute gear is obtained.

2. Synthesis and Reconstruction of Error Tooth Surface

The sum of the deviation values of the normal direction at the corresponding contact point on the tooth surface is called the synthesis error. In this paper, a grinding method with high grinding precision is used to grind the gear. This method is through the grinding wheel to grind the gear, and then get the relevant tooth shape. When the standard gear is ideally engaged, the contact line will cover the entire tooth surface, which is called the geometric contact line. This line also serves as the reference for the contact position. The tooth surface error is defined as the size of the angle in the normal direction when the actual tooth surface corresponds to the reference plane.

2.1. Synthesis of Error Tooth Surface. In this paper, a base section of the gear is divided into 20 equal parts for gear contact analysis. The ideal contact part for the different size of gears is shown in Figure 1.

The interval between the contact lines is one twentieth of the rotation angle of a base section. The contact lines on the tooth surface of the large gear are numbered with $i = 1, 2, \ldots, N$ (N is the total number of contact lines) in the order of start contact to the end of the contact. The length of a contact line is divided into 19 equal parts, and the corresponding division points are numbered with $j = 1, 2, \ldots, 20$ in the order of the tooth root to the tooth top. The tooth surfaces meshing with the large gears are divided by the same method. Therefore, the reference plane position on the different size of gears can be expressed by the combination of the serial number of the contact line i and the division number j of the contact line. The shape deviation of the gear can be expressed as data $20 \times n$.

The sum of the deviation values of the normal direction at the corresponding contact point on the tooth surface is called the synthesis error. The curve of the 20 synthetic error values on a geometric contact line is called the synthetic error curve. In this paper, the synthetic error surface is expressed in a coordinate system with the split number j of a geometric contact line being the X-axis and the contact line number i is the plane of the Y axis, which is shown in Figure 2. The direction of the synthetic error coordinate system e is positive and the highest point is zero. The minimum of the synthetic error on the geometric contact line is defined as the ridge. The projection of the ridge to the synthetic error coordinate system Y-e surface is called the ridge shape.

2.2. Tooth Surface Model Based on NURBS. NURBS surface is the only representation standard of product data model defined in STEP standard (Product data exchange standard), and it has been applied in real tooth surface simulation. However, in the process of real tooth surface reconstruction by using NURBS surface, the precision of the reconstructed tooth surface in the nongrid node is difficult to control due to the limited number of measurement data points. In order to ensure the smoothness of reconstructed tooth surface, this paper proposes a linear interpolation method combined with area weight interpolation method. This method is used to estimate the tooth surface data points which are outside the measurement area to realize the construction of the error tooth surface and to ensure the accuracy of the reconstructed tooth surface to the utmost extent.

NURBS surfaces are tensor product forms based on NURBS curves, and the double three NURBS surface can be expressed as

$$P(u,v) = \frac{\sum_{i=1}^{m}\sum_{j=1}^{n} B_{i,k}(u)\, B_{j,k}(v)\, \omega_{ij} V_{ij}}{\sum_{i=1}^{m}\sum_{j=1}^{n} B_{i,k}(u)\, B_{j,k}(v)\, \omega_{ij}} \qquad u, v \in [0,1], \tag{1}$$

where m is the number of control vertices for u, n is the number of control vertices for v, and V_{ij} is the control vertex of the surface. ω_{ij} is the weight factor of V_{ij}. $B_{i,k}$ is the kth spline basis function along u. $B_{j,k}$ is the kth spline basis function along v. Among them, the basis function recursive formula is

$$B_{i,0}(u) = \begin{cases} 1 & u_i \le u \le u_{i+1} \\ 0 & \text{other} \end{cases}$$

$$B_{i,k}(u) = \frac{u - u_i}{u_{i+k} - u_i} B_{i,k-1}(u) + \frac{u_{i+k+1} - u}{u_{i+k+1} - u_{i+1}} B_{i+1,k-1}(u) \quad k \ge 1. \tag{2}$$

2.3. Delaunay Triangulation of Discrete Data. In this paper, the scanning method is used to obtain the tooth surface discrete point data. In order to describe the real tooth surface situation more intuitively, this paper deals with the discrete data points by means of Delaunay triangulation principle because the topological relations between the discrete data points are complex. The traditional Delaunay triangulation method often projects the three-dimensional discrete data points onto the two-dimensional plane and then triangles the projection points. However, the triangulation of this method cannot truly reflect its spatial angle, which will affect the quality of the section. On the basis of these methods, this paper presents a method of direct triangulation of three-dimensional discrete data points.

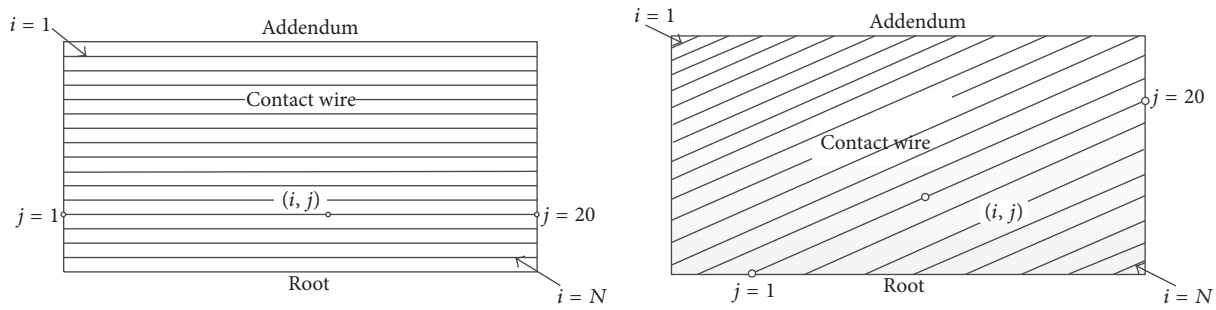

(a) The ideal contact part for spur gears

(b) The ideal contact part for helical gears

Figure 1: The geometrical contact line of the tooth surface during the meshing process. i: the corresponding contact line number during the engagement process; j: split points on the contact line.

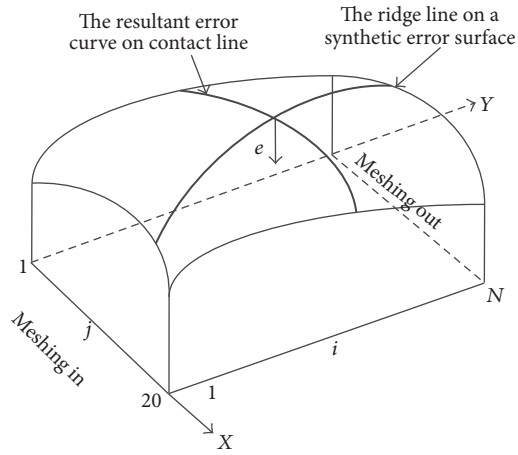

Figure 2: The creation of synthetic error surfaces.

Assuming that the scan line is ℓ_i, $k = 1, 2, \ldots, n$, the number of measurement points on the scan line is t, where two adjacent scanning lines are ℓ_k, ℓ_{k+1}, $1 \le k < k+1 \le n$. The measurement points on each of the two scanning lines are $\ell_k(j)$, $j = 1, 2, \ldots, t$; $\ell_{k+1}(l)$, $l = 1, 2, \ldots, t$.

As shown in Figure 3, the starting points for connecting two scan lines are $\ell_k(1)$ and $\ell_{k+1}(1)$; the end point are $\ell_k(t)$ and $\ell_{k+1}(t)$. And find another scan line that is closest to the measurement point in the measurement points on ℓ_k and ℓ_{k+1} and connect, where the area between the scanning lines ℓ_k and ℓ_{k+1} is divided into r $(r \ge t-1)$ spatial regions. Finally, the triangular and spatial quadrilateral regions are retrieved.

For the spatial quadrilateral region, the minimum internal angle maximum criterion is used to complete the Delaunay triangulation of the discrete data points in this paper, respectively, as shown in Figure 4.

2.4. Linear Interpolation Method and Area Weight Interpolation Method. In order to describe the error of the tooth surface quickly and accurately, it is necessary to block the discrete data points of the tooth surface in the construction of the digital real tooth surface. And use the interpolation method to accurately describe the error surface to reduce the amount of tooth interpolation calculation. The traditional data block method is often based on the geometric characteristics of the part, which does not apply to free surfaces that describe the error tooth surface. In this paper, an interpolation method based on linear interpolation combined with area weight interpolation is proposed to accurately identify tooth surface errors.

The error tooth surface shape is calculated by using the area weight method according to the following interpolation method. In Figure 5, assume that A, B, C, D are the measurement points and the tooth surfaces of these points have been determined, and the data of point O can be obtained. Firstly, calculate the 4 points around point for linear interpolation. The value of the point O surrounded by point A, B, C, D is calculated by using the area weights of the interpolation values of the four triangles ABC, BCD, ABD, ACD. If point O is close to a region, the area weighting factor is close to one. If point O is far from the area, the area weighting factor is close to zero. When the interpolation point coincides with the measurement point, the interpolation value is the measured value itself.

As shown in Figure 5, assumptions are as follows: the linear interpolation value where the triangles ABC pass through the interpolation point O is a_1; the area of triangle ABC is S_{ACOB}, The interpolation value of triangle BCD is

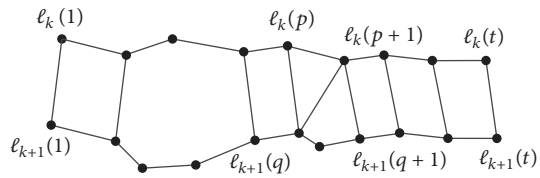

Figure 3: Preliminary Delaunay triangulation of adjacent tooth surface scan lines.

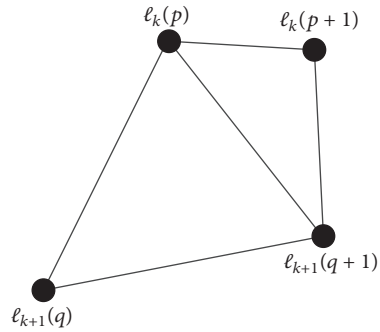

Figure 4: Polygon area triangulation.

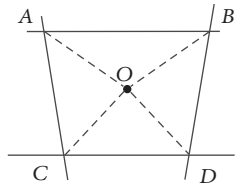

Figure 5: Four-point interpolation algorithm.

a_2; the area of triangle BCD is S_{OCDB}. Thus the interpolation value is b_1.

$$b_1 = \frac{S_{ACOB}}{S_{ACDB}} a_2 + \frac{S_{OCDB}}{S_{ACDB}} a_1, \tag{3}$$

where S_{ACDB} is the area of quadrilateral $ABCD$.

On the other hand, the triangular ABD and ACD's interpolation values for point O are a_3, a_4 and the triangular ABD and ACD's areas are S_{OABD}, S_{ACDO}, respectively. Thus the interpolation value is b_2.

$$b_2 = \frac{S_{OABD}}{S_{ACDB}} a_4 + \frac{S_{ACDO}}{S_{ACDB}} a_3. \tag{4}$$

The final interpolation value b is

$$b = \frac{b_1 + b_2}{2}. \tag{5}$$

3. The Simulation of Contact Pattern

3.1. The Basic Theory of Contact Parts. When the tooth surface is transferring load, the contact tooth surface will be elastically deformed so that the area around the contact part will make contact. As the teeth continue meshing, the area left of the tooth surface is the actual tooth contact area, as shown in Figure 6.

3.2. Analytical Method of Contact Part of Involute Gear. As shown in Figure 7, σ_{0i} $(i = 1, 2)$ represents two coordinate systems whose origin is O_1, O_2. k_{oi} coincides with i axis of the gear coordinate system, $\overline{O_1O_2} = E$ is the gear offset distance, and j_{oi} coincides with the vertical axis of the two axes. The two gears are rotated φ_1, φ_2 angles, respectively. The coordinate systems are σ_1, σ_2, respectively. A coordinate system $\sigma_M(M; \alpha_\varsigma, \alpha_\eta, n)$ is established at the contact point M of the tooth surface Σ_2, where n is the unit normal vector at point M on the tooth surface Σ_2. α_ς and α_η are two vertical unit vectors at the contact point M of the tooth face Σ_2. Take any node Q_2 on the tooth face Σ_2. And draw a straight line from this point Q_2 along a normal direction n to the tooth surface Σ. Then get the intersection Q_1 of the straight line and the tooth surface Σ_1.

Coordinate transformation matrix $\sigma_2 \to \sigma_M$ is

$$[T_{2M}] = \begin{bmatrix} a_{11} & a_{12} & a_{13} \\ a_{21} & a_{22} & a_{23} \\ a_{31} & a_{32} & a_{33} \end{bmatrix}, \tag{6}$$

where $a_{11} = \alpha_\varsigma \cdot i_2$, $a_{12} = \alpha_\varsigma \cdot j_2$, $a_{13} = \alpha_\varsigma \cdot k_2$, $a_{21} = \alpha_\eta \cdot i_2$, $a_{22} = \alpha_\eta \cdot j_2$, $a_{23} = \alpha_\eta \cdot k_2$, $a_{31} = n \cdot i_2$, $a_{32} = n \cdot j_2$, $a_{33} = n \cdot k_2$.

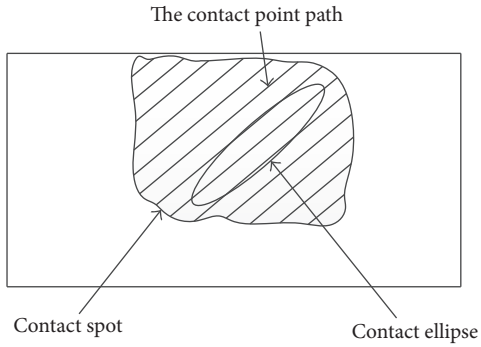

Figure 6: Schematic diagram of contact parts.

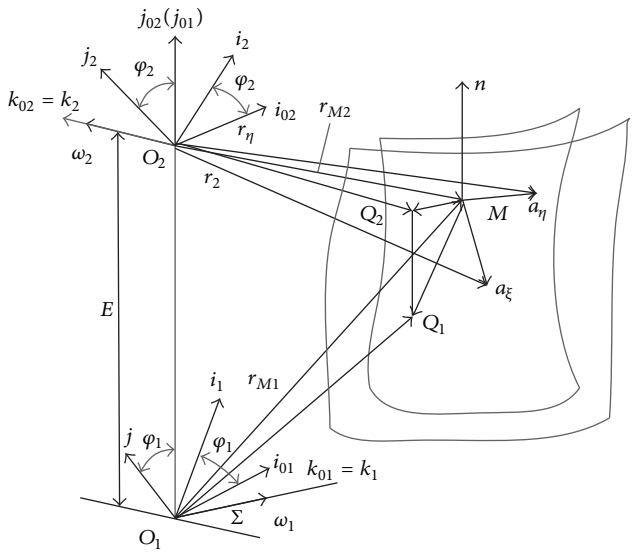

Figure 7: Conversion diagram of tooth surface meshing coordinate system.

According to Figure 7

$$[T_{2M}] = \begin{bmatrix} -\cos\Sigma & 0 & -\sin\Sigma \\ 0 & 1 & 0 \\ \sin\Sigma & 0 & -\cos\Sigma \end{bmatrix}. \tag{7}$$

Thus Coordinate transformation matrix $\sigma_2 \to \sigma_M$ is

$$\begin{aligned} [T_{1M}] &= [T_{2M}] \cdot R[k_2, -\varphi_2] \cdot R[j_{O2}, 180^\circ + \Sigma] \cdot R[k_{O1}, \varphi_1] \\ &= [T_{2M}] \begin{bmatrix} \cos\varphi_2 & \sin\varphi_2 & 0 \\ -\sin\varphi_2 & \cos\varphi_2 & 0 \\ 0 & 0 & 1 \end{bmatrix} \begin{bmatrix} -\cos\Sigma & 0 & -\sin\Sigma \\ 0 & 1 & 0 \\ \sin\Sigma & 0 & -\cos\Sigma \end{bmatrix} \begin{bmatrix} \cos\varphi_1 & -\sin\varphi_1 & 0 \\ \sin\varphi_1 & \cos\varphi_1 & 0 \\ 0 & 0 & 1 \end{bmatrix}, \end{aligned} \tag{8}$$

where $R[k_2, -\varphi_2]$ is the coordinate transformation matrix of $\sigma_2 \to \sigma_M$; $R[j_{O2}, 180^\circ + \Sigma]$ is the coordinate transformation matrix of $\sigma_{O1} \to \sigma_{O2}$.

$R[k_{O1}, \varphi_1]$ is the coordinate transformation matrix of $\sigma_1 \to \sigma_{O1}$.

The vector diameter of point Q_2 in the coordinate system σ_M is

$$\begin{aligned} (r_{O2})_M &= (r_2)_M + (M_{O2})_M \\ &= [T_{2M}](r_2)_2 + [T_{2M}](M_{O2})_2. \end{aligned} \tag{9}$$

The vector diameter of point Q_1 in the coordinate system σ_M is

$$\begin{aligned}(r_{O1})_M &= (r_1)_M + (M_{O1})_M \\ &= (r_1)_M + (M_{O2})_M + (O_1O_2)_M,\end{aligned} \tag{10}$$

where $(r_2)_2$ is the r_2 vector in coordinate system σ_2 and $(M_{O2})_2$ is a vector of point O_2 to point M in coordinate system σ_2. $(r_1)_M$ is the r_1 vector in coordinate system σ_M. $(M_{O2})_M$ is a vector of point O_2 to point M in coordinate system σ_M. $(O_1O_2)_M$ is a vector of point O_1 to point O_2 in coordinate system σ_M. The expression of vector $(O_1O_2)_M$ is

$$(O_1O_2)_M = [T_{2M}]\, R\,[k_2, -\varphi_2] \begin{bmatrix} 0 \\ -O_1O_2 \\ 0 \end{bmatrix}, \tag{11}$$

where $R[k_2, -\varphi_2]$ is the coordinate transformation matrix of $\sigma_2 \to \sigma_M$.

In coordinate system σ_M, the projection for difference between MQ_2 and MQ_1 in the normal vector direction n_1 at the point M on the tooth surface Σ_2 is the clearance in the direction of the engagement of the two tooth surfaces at the point Q_1 and point Q_2. When the pinion turns through angle φ_1, the gear turns through angle φ_2:

$$\begin{aligned}(r_{Q1})_M &= \{x_{Q1}, y_{Q1}, z_{Q1}\} \\ (r_{Q2})_M &= \{x_{Q2}, y_{Q2}, z_{Q2}\}.\end{aligned} \tag{12}$$

In order to ensure that the point Q_2 on the tooth surface Σ_2 of the large gear is still the point Q_1 on the tooth surface Σ_1 of the pinion in the direction of n, the vectors r_{Q1} and r_{Q2} must satisfy the following relationships:

$$\begin{aligned}x_{Q2} - x_{Q1} &\le 10^{-4} \\ y_{Q2} - y_{Q1} &\le 10^{-4}.\end{aligned} \tag{13}$$

The clearance between the two engaging tooth surfaces Σ_1 and Σ_2 in the direction of n at points Q_1 and point Q_2 is

$$\Delta z = \overline{Q_1Q_2} = z_{Q2} - z_{Q1}. \tag{14}$$

According to GB/Z18620.4-2008, the thickness of the detection coating for contact part is set to 0.01 mm. The light load contact part exists in the area of contact point separation amount $\delta_1 = 0.01$ mm. When $\Delta z \le 0.01$ mm, it is considered that the two tooth surfaces Σ_1 and Σ_2 are in contact at point Q_1 and point Q_2. By dividing the tooth surface into the grid, the clearance in the direction of n the corresponding grid node is calculated, so is the tooth contact part.

4. Prediction of Dynamic Performance of Error Tooth Surface

The main causes of gear vibration are gear manufacturing error, installation error, gear time varying meshing stiffness and load gear, shaft, gearbox, and other deformation caused by the gear position error. The gear contact part and transmission error is the visualization of gear meshing performance. In the example, the reliability of the prediction results is judged by measuring the vibration of the gears in the direction of the meshing line.

4.1. Gear Transmission Error. The factors that affect the dynamic excitation of the gear are not only the structural form of the gear itself, the geometric characteristics, and the error, but also the other components in the system. The cylindrical gear system can be simplified as a torsional vibration system for the gear pair when the stiffness of the support member such as the drive shaft, bearing, and housing is large. The dynamics model is shown in Figure 8.

Suppose the gear pair of coincidence between one and two. According to the mechanical dynamics theory and the mechanical vibration theory, the torsional vibration equation of a pair of gear pair is

$$M\frac{d^2x}{dt^2} + c_m\frac{dx}{dt} + k_m x = W_0 + W_d, \tag{15}$$

where

$$\begin{aligned}x &= r_1\theta_1 - r_2\theta_2 \quad M = I_1I_2/\left(I_1r_2^2 + I_2r_1^2\right) \\ W_0 &= \frac{T_1}{r_1} = \frac{T_2}{r_2} \\ W_d &= k_1e_1 + k_2e_2 + c_1\frac{de_1}{dt} + c_2\frac{de_2}{dt}.\end{aligned} \tag{16}$$

In the above formula,

θ_i $(i = 1, 2)$ is the torsional vibration displacement of gear and pinion.

I_i $(i = 1, 2)$ is the inertia of the gear and pinion.

r_i $(i = 1, 2)$ is the base radius of the gear and pinion.

k_i $(i = 1, 2)$ is the integrated stiffness of the pair of ith gears.

c_i $(i = 1, 2)$ is the damping coefficient of the ith gear.

$k(t)$ is the combined meshing stiffness of gear pair.

c is meshing damping of gear pair.

e_i $(i = 1, 2)$ is the error of the ith gear.

T_i $(i = 1, 2)$ is the external load moment on the driving and driven gears.

When the dynamic term such as inertia force and damping force term is ignored, the static transmission error is

$$x_s = \frac{W_0}{k(t)} + \frac{(k_1e_1 + k_2e_2)}{k(t)}. \tag{17}$$

In the quasi-static transmission error test of the gear pair, it is necessary to know exactly the rotation angle of the driving and driven gears in the transmission process.

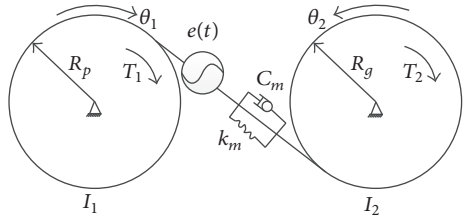

Figure 8: Torsional vibration model of gear pair.

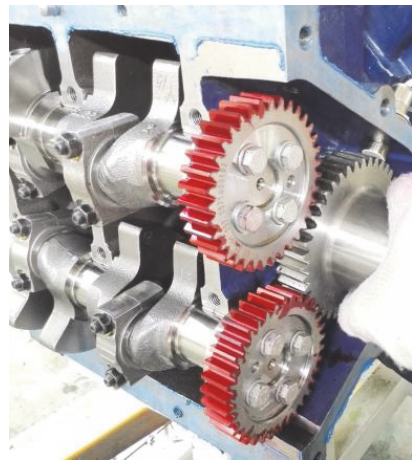

Figure 9: Gear distribution diagram.

Table 1: Factors and their levels.

Parameters	Letter symbols	
Gear modulus	m	2.5
Pressure angle	α	20
Addendum	h_a	2.5
Dedendum	h_f	3.125
Teeth	Z	35/42

5. Experiment Study

This paper chooses the gears of a certain type of solar generator gearbox to carry on the research. According to the support stiffness of the gear and other factors, refer to optimizing the gear modification [11–27]. This paper would not study the best trimming tooth surface; that is, select two measurements modification gears; it is short for group A and group B in the following paper, and its dynamic performance in analysis.

The transmission mechanism in the gearbox is composed of three spur gears, and the structure of the gearbox is shown in Figure 9. The two gears with 35 teeth are the pinion gear, and the gears with the number of teeth are 42. The speed of the drive wheel is 1800 r/min and the rated power is 25 KW. The basic parameters of the gear are shown in Table 1.

Using the measurement method of ZEISS coordinate measuring instrument, the topological measurement of tooth width and tooth height is taken. According to the actual measurement data, the surface of the tooth surface deviation is directly constructed, and the shape deviation surface in the measurement area of the two sets of gear driving wheels is shown in Figure 10. Through the calculation of the points of the measurement area through the interpolation algorithm, tooth surface with the shape deviation on the different mesh nodes is obtained, which are shown in Figure 11.

On the basis of the analysis of the contact part of the error tooth surface after interpolation, the contact surface of the tooth surface is shown in Figure 12.

The theoretical calculation of the transmission error is shown in Figure 13.

A gear loading test is performed for gears whose tooth surfaces are coated with steel red after steel red is dried, and the gear contact parts are shown in Figure 14, The transmission error of the gear is shown in Figure 15.

In order to test the accuracy of the structural error surface, the vibration measuring instrument is used to measure the time-domain diagram of the vibration in the direction of the gear meshing line, and its FFT is shown in Figure 16.

It can be seen from the figure that the predictive gear contact part and gear transmission error is basically the same as test results. The vibration measurement of the gearbox along the gear meshing line shows that the vibration condition of the gearbox is basically the same as the transmission error of the gear. This shows that the model of error tooth surface is accurate.

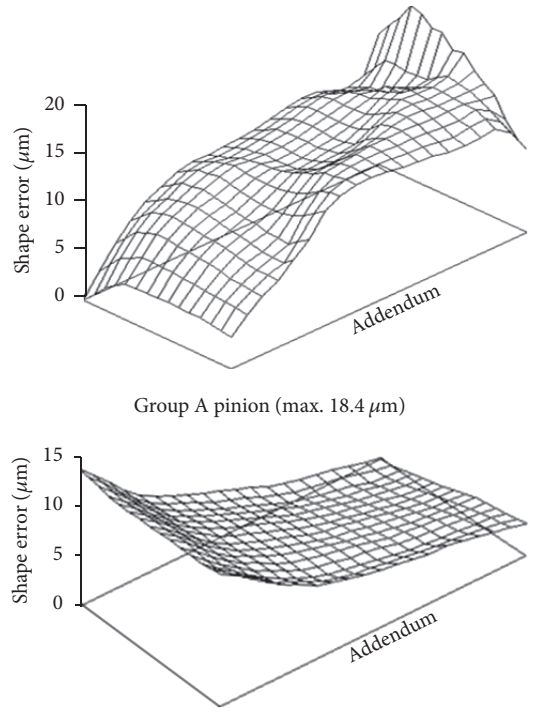

Figure 10: The tooth surface with shape deviation in the measurement area.

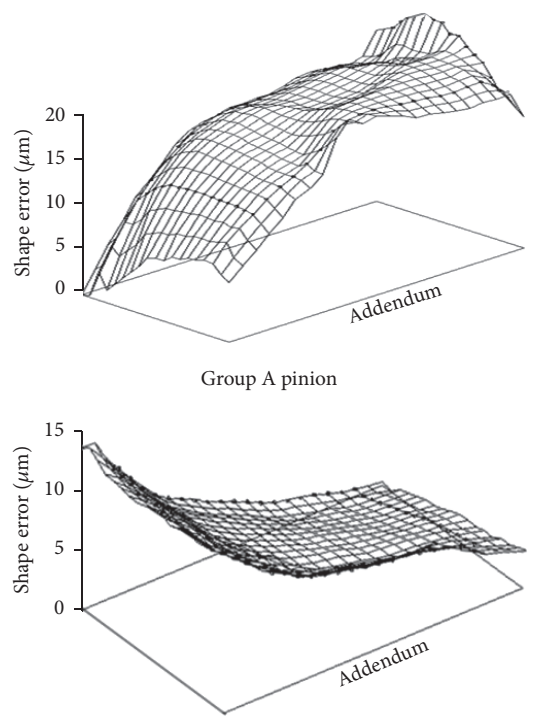

Figure 11: The tooth surface with shape deviation in the measurement area after interpolation.

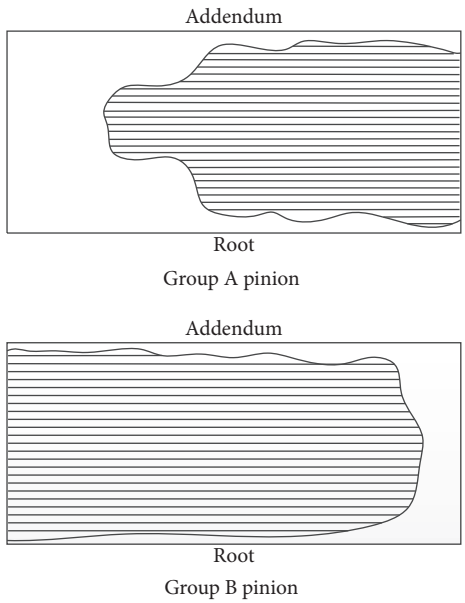

Figure 12: Tooth surface contact parts (theoretical calculation).

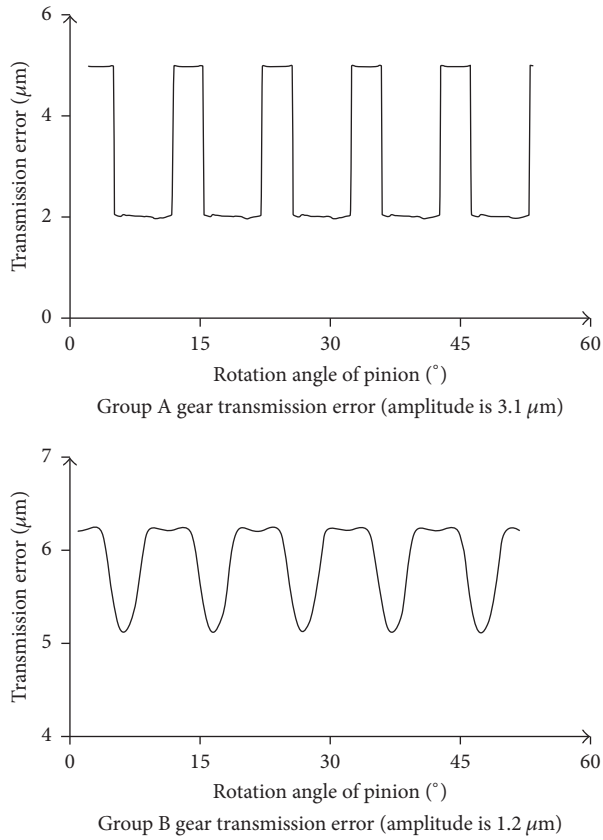

Figure 13: Gear drive error (theoretical calculation).

6. Conclusions

(1) An algorithm combining linear interpolation with area weight interpolation is proposed to realize the construction of error tooth surface. This method not only reduces the computational complexity of the tooth surface interpolation algorithm, but also improves the efficiency of the digital tooth surface construction.

(2) The contact part and the transmission error of the gear are analyzed by using the constructed error tooth

Group A pinion

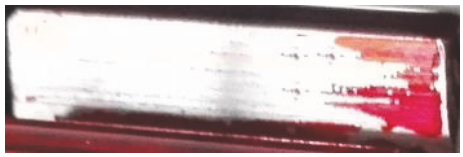

Group B pinion

Figure 14: Contact part of test gear.

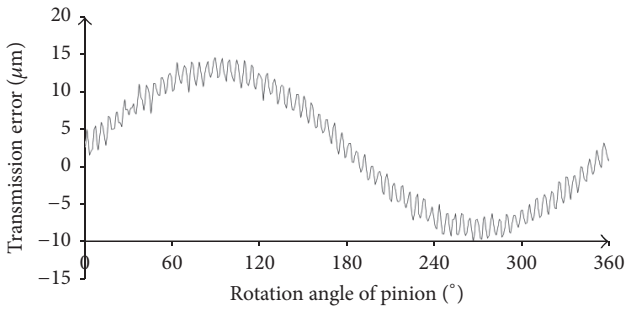

Group A gears (amplitude is 3.5 μm)

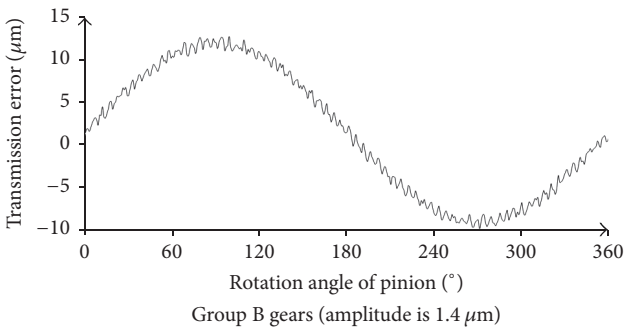

Group B gears (amplitude is 1.4 μm)

Figure 15: Transmission error of test gear.

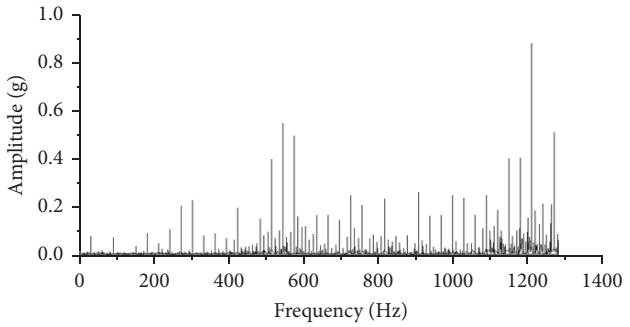

Group A (the maximum value is 0.88)

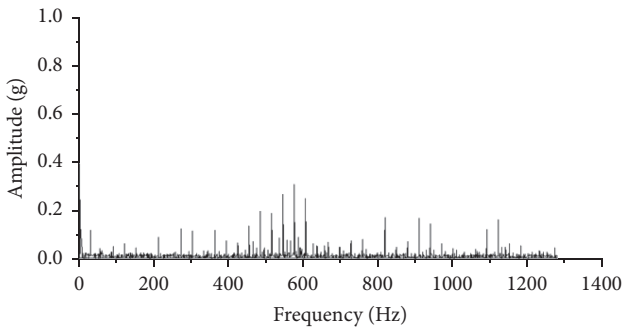

Group B (the maximum value is 0.3)

Figure 16: Gearbox vibration spectrum.

surface, which provides a new idea for the prediction of the dynamic performance of the gear.

(3) Through the gear loading test, the contact part and gear transmission error of the gear are obtained. The analysis result and the test result are basically the same, which shows the accuracy of the constructed error tooth surface.

(4) The construction of the error tooth surface in this paper lays the foundation for further improving the grinding accuracy of the tooth surface and the grinding of the high performance gear.

Nomenclature

V_{ij}: Control vertex of the surface
ω_{ij}: Weight factor of V_{ij}
$B_{i,k}$: kth spline basis function along u
$B_{j,k}$: kth spline basis function along v
T_i $(i = 1, 2)$: External load moment on the driving and driven gears
$k(t)$: Combined meshing stiffness of gear pair
c: Meshing damping of gear pair
e_i $(i = 1, 2)$: the error of the ith gear.

Conflicts of Interest

The authors declare that there are no conflicts of interest regarding the publication of this paper.

Acknowledgments

The authors would like to thank Shanghai Science and Technology Commission (Science and Technology Support

Program for the People's Livelihood) for the process adaptability test and evaluation and application on NC equipment manufacturing for aerospace complex structural parts, Grant no. 15110502300.

References

[1] S. Zhou, G. Song, Z. Ren, and B. Wen, "Nonlinear dynamic analysis of coupled gear-rotor-bearing system with the effect of internal and external excitations," *Chinese Journal of Mechanical Engineering*, vol. 29, no. 2, pp. 281–292, 2016.

[2] J. Lin, Z. Shi, C. Pan, and B. Zhang, "Profile error evaluation of large gears based on NURBS surface fitting," *Yi Qi Yi Biao Xue Bao/Chinese Journal of Scientific Instrument*, vol. 37, no. 3, pp. 533–539, 2016.

[3] J.-H. Zhang, Z.-D. Fang, and C. Wang, "Digital simulation of spiral bevel gears' real tooth surfaces based on non-uniform rational B-spline," *Hangkong Dongli Xuebao/Journal of Aerospace Power*, vol. 24, no. 7, pp. 1672–1676, 2009.

[4] G. Li, Z. Wang, Z. Geng, and W. Zhu, "Modeling approach of digital real tooth surfaces of hypoid gears based on non-geometric-feature segmentation and interpolation algorithm," *Jixie Gongcheng Xuebao/Journal of Mechanical Engineering*, vol. 51, no. 7, pp. 77–84, 2015.

[5] D. Sun, X. Li, Y. Li, and Z. Tian, "G1-continuous algorithms of triangular mesh surface," *Jixie Gongcheng Xuebao/Journal of Mechanical Engineering*, vol. 46, no. 15, pp. 125–129, 2010.

[6] Z. H. Wang, Simulation of hypoid gears dynamic performance, 2013.

[7] Z. Wang, A. Kubo, S. Asano, S. Kato, and T. Nonaka, "Simulation of deterioration of hypoid gear performance due to tooth flank wear (2nd report. model for tooth flank wear and the change of gear performance resulted)," *Transactions of the Japan Society of Mechanical Engineers*, vol. 66, no. 647, pp. 2363–2370, 2000.

[8] G. Li, Z. Wang, and A. Kubo, "The modeling approach of digital real tooth surfaces of hypoid gears based on non-geometric-feature segmentation and interpolation algorithm," *International Journal of Precision Engineering and Manufacturing*, vol. 17, no. 3, pp. 281–292, 2016.

[9] Z. Wang, A. Kubo, and T. Nonaka, "Prediction of performance of hypoid gears by observation of tooth contact pattern (1st report, algorithm for predicting composite error surface)," *TRansactions of the Japan Society of Mechanical Engineers*, vol. 64, no. 624, pp. 3103–3111, 1998.

[10] Z. Wang, A. Kubo, S. Asano, S. Kato, and T. Nonaka, "Simulation of deterioration of hypoid gear performance due to tooth flank wear. 1st report, data processing of measured tooth flank form deviation for performance simulation," *Transactions of the Japan Society of Mechanical Engineers*, vol. 66, no. 647, pp. 2354–2362, 2000.

[11] S. Chen, J. Tang, Z. Wang, and Z. Hu, "Effect of modification on dynamic characteristics of gear transmissions system," *Jixie Gongcheng Xuebao/Journal of Mechanical Engineering*, vol. 50, no. 13, pp. 59–65, 2014.

[12] Y.-Z. Sun, R.-P. Zhu, and H.-Y. Bao, "Calculation of mean friction coefficient in scuffing strength for gear drive with meshing beyond pitch point," *Hangkong Dongli Xuebao/Journal of Aerospace Power*, vol. 28, no. 9, pp. 2155–2160, 2013.

[13] L. Chang, Y.-R. Jeng, and P.-Y. Huang, "Modeling and analysis of the meshing losses of involute spur gears in high-speed and high-load conditions," *Journal of Tribology*, vol. 135, no. 1, Article ID 011504, 2013.

[14] M. Vaishya and R. Singh, "Strategies for modeling friction in gear dynamics," *Journal of Mechanical Design*, vol. 125, no. 2, pp. 383–393, 2003.

[15] S. Li and A. Kahraman, "A tribo-dynamic model of a spur gear pair," *Journal of Sound and Vibration*, vol. 332, no. 20, pp. 4963–4978, 2013.

[16] S. Li, "Effects of misalignment error, tooth modifications and transmitted torque on tooth engagements of a pair of spur gears," *Mechanism and Machine Theory*, vol. 83, pp. 125–136, 2015.

[17] T. J. Lisle, B. A. Shaw, and R. C. Frazer, "External spur gear root bending stress: a comparison of ISO 6336:2006, AGMA 2101-D04, ANSYS finite element analysis and strain gauge techniques," *Mechanism and Machine Theory*, vol. 111, pp. 1–9, 2017.

[18] J. Tang, H. Chen, and Q. Wang, "Dynamics model of gear transmission with combined friction and clearance by using bond graph method," *Jixie Gongcheng Xuebao/Journal of Mechanical Engineering*, vol. 47, no. 9, pp. 53–59, 2011.

[19] J. I. Pedrero, M. Pleguezuelos, and M. Muñoz, "Critical stress and load conditions for pitting calculations of involute spur and helical gear teeth," *Mechanism and Machine Theory*, vol. 46, no. 4, pp. 425–437, 2011.

[20] M. Miladi Chaabane, R. Plateaux, J.-Y. Choley, C. Karra, A. Riviere, and M. Haddar, "Topological modeling of a one stage spur gear transmission," *Chinese Journal of Mechanical Engineering*, vol. 27, no. 5, pp. 900–908, 2014.

[21] M. H. Jia, C. L. Wang, and B. Ren, "Manufacturing error effects on mechanical properties and dynamic characteristics of rotor parts under high acceleration," *Chinese Journal of Mechanical Engineering*, vol. 30, no. 4, pp. 920–932, 2017.

[22] V. V. Simon, "Micro tooth surface topography of face-milled hypoid gears," *Mechanism and Machine Theory*, vol. 104, pp. 370–381, 2016.

[23] V. V. Simon, "Optimal machine-tool settings for the manufacture of face-hobbed spiral bevel gears," *Journal of Mechanical Design*, vol. 136, no. 8, Article ID 081004, 2014.

[24] H. Ding, J. Tang, Y. Zhou, J. Zhong, and G. Wan, "A multi-objective correction of machine settings considering loaded tooth contact performance in spiral bevel gears by nonlinear interval number optimization," *Mechanism and Machine Theory*, vol. 113, pp. 85–108, 2017.

[25] H. Ding, J. Tang, and J. Zhong, "An accurate model of high-performance manufacturing spiral bevel and hypoid gears based on machine setting modification," *Journal of Manufacturing Systems*, vol. 41, pp. 111–119, 2016.

[26] A. Artoni, A. Bracci, M. Gabiccini, and M. Guiggiani, "Optimization of the loaded contact pattern in hypoid gears by automatic topography modification," *Journal of Mechanical Design*, vol. 131, no. 1, pp. 0110081–0110089, 2009.

[27] A. Artoni and M. Guiggiani, "Revisiting generation and meshing properties of beveloid gears," *Journal of Mechanical Design*, vol. 139, no. 9, pp. 1–9, 2017.